DISCHARGE CHARACTERISTICS OF DIELECTRIC MATERIALS EXAMINED IN MONO-, DUAL-, AND SPECTRAL ENERGY ELECTRON CHARGING ENVIRONMENTS*

P. Coakley, M. Treadway, N. Wild, and B. Kitterer
Jaycor
San Diego, California 92138

1. INTRODUCTION

In an effort to explain the effects of mid-energy electrons (25 to 100 keV) on the charge and discharge characteristics of spacecraft dielectric materials and expand the data base from which basic discharge models can be formulated, thin dielectric materials were exposed to low- (1 to 25 keV), mid- (25 to 100 keV), combined low- and mid-, and spectral- (1 to 100 keV) energy electron environments. This effort has produced three important results. First, it has determined electron environments that lead to dielectric discharges at potentials less negative than -5 kV. Second, this effort has identified two types of discharges that appear to dominate the kinds of discharges seen: those with peak currents, $I \gg 10$ A and pulse widths, $\tau > 300$ ns, and those with $I < 5$ A and $\tau < 20$ ns. Third, this effort has shown that, for the thin dielectric materials tested, the worst-case discharges observed in the various environments are similar.

Previous laboratory experiments have focused on the effects of monenergetic low-energy electron charging and discharging of various spacecraft dielectric materials (Ref. 1). These experiments showed that, for samples with electrically-grounded substrates, discharges occurred only when surface potentials exceeded -5 kV. The discharges blew off more than 30% of the stored charge (Ref. 2) and the pulse widths of the discharge currents scaled in size as the square root of the sample area (Ref. 3). The discharges brought the sample's surface potential down generally less negative than -5 kV. For samples comparable in area and thickness to the samples that we tested, the pulse amplitudes were much greater than 10 A and the pulse widths equaled or exceeded 300 ns. These laboratory data are in apparent disagreement with satellite data that indicate for satellites in geosynchronous altitude environments, discharges occur when surface potentials are less than -2 kV (Refs. 4 and 5). Furthermore, data from ATS5 and ATS6 indicate that discharges occur in bunches and that as many as 80 discharge events have occurred in a single hour (Ref. 6). This latter observation implies that discharges on satellites may not cleanse the entire surface of stored charge and perhaps occur as small localized events.

This paper discusses the results of our monenergetic, dual-energy and spectrum-energy electron tests performed on seven dielectric samples: Teflon, Optical Solar Reflector (OSR), Alphaquartz, Kapton, perforated Kapton, Mylar, and a "nude" Space Transportation System (STS) tile. Section 2 describes the experimental apparatus and electron simulation environment. Section 3 discusses the general trends found in the data, comparing the samples with each other with emphasis on the four electron environments: monoenergetic low-, monoenergetic mid-, dual-, and spectrum-energy electrons. Finally, in Section 4 we present conclusions.

*Work sponsored by the Air Force Weapons Laboratory and NASA Lewis Research Center under Contract No. F29601-82-C-0015.

2. EXPERIMENTAL APPARATUS AND ELECTRON-SIMULATION ENVIRONMENT

The experiments were performed in a 1.3-m long, 1.3-m diameter vacuum chamber, shown in Figure 1. Thirty-cm diameter test samples were positioned 20 cm off the door at one end of the chamber, and two Kimball Physics monoenergetic-electron guns pointed toward the samples. Pressures in the test chamber during experimental tests measured in the mid 10^{-7} torr regime. The energy of one of the two guns ranged from 1 to 100 keV, whereas the range of the other gun went from 1 to 25 keV. The maximum current output of the two guns measured 400 μA. For sample exposure tests the beam current density measured in the plane of the test sample was generally held between 0.03 and 3 nA/cm^2. For monoenergetic exposure tests the beam of each gun was rastered over the entire sample end of the chamber using pairs of the Helmholtz coils driven with alternating currents at frequencies of 60 Hz horizontal and 103 Hz vertical. The rastered beams produced a time-averaged flux across the sample, uniform to within ±15% for electrons from the low-energy gun and to within ±7% for electrons from the mid-energy gun.

2.1 SPECTRAL SOURCE

Our electron spectral source used the two Kimball Physics electron guns and two high-voltage biased disc-shaped scattering foils. Each scattering foil consisted of several thicknesses of aluminum sheets, ranging in size from 0.04 mils to 2.0 mils thick, and configured as wedges to a pie. Monoenergetic electrons incident on a thin foil lose energy and intensity as they scatter through the foil, depending on the relative thickness of each aluminum scatterer. The average scattered electron energy $\langle E_s \rangle$ approximately equals the average energy lost, $dE/dX|_{E_0}$, times a foil thickness, ΔX, and subtracted from the incident electron energy E_0,

$$\langle E_s \rangle = E_0 - dE/dx|_{E_0} \cdot \Delta X \ . \tag{1}$$

The average scattered electron energy has nearly a linear dependence on foil thickness and a weak functional dependence on average energy lost [i.e., dE/dX depends weakly on E_0 (Ref. 7)]. The electron transmission intensity has a power series dependence on the foil thickness or incident electron energy. The thinner the foil or the higher the incident electron energy, then the greater the transmitted electron intensity.

By adding a high-voltage bias, V, to the scattering foil, one then has for the average scattered electron energy

$$\langle E_s \rangle = (E_0 + V) - (dE/dX|_{E_0+V}) \cdot \Delta X - V \tag{2}$$

or

$$\langle E_s \rangle = E_0 - (dE/dX|_{E_0+V}) \cdot \Delta X \ . \tag{3}$$

Any electrons incident on the scattering foil pick up an energy, V, when they hit the foil. With a total energy of $E_0 + V$ they scatter through the foil. They give up the added potential energy V (the last term in Eq. 2) when they pass close to any grounded surface, e.g., a test sample. Compared with the unbiased foil, the scattered electron energy changes by a small amount since it depends weakly on $dE/dX|_{E_0+V}$, whereas the scattered electron intensity becomes greatly enhanced.

This high-voltage bias technique makes an impact when one tries to produce 1- to 10-keV scattered electrons using an incident 16-keV electron beam and when trying to produce 12- to 30-keV scattered electrons using an incident 85-keV electron beam. Without high-voltage bias, it becomes next to impossible to produce a flux of scattered 1- to 5-keV electrons with an incident electron beam of 10 keV or above, due to the attenuation of the incident beam in the foil. We enhanced the flux by an order of magnitude when exposing a 0.22-mil foil with 16-keV electrons (comparing results with and without a 15-kV foil bias).

Figure 2 shows a graph of Spectrum 1, dN/dE = const., that was produced using the high-voltage biased foil technique. The multiple curves at the bottom of the graph are the scattered electron spectra produced from each given foil thickness and area. There were 16-keV electrons incident on the 0.22-mil, 0.16-mil, 0.12-mil, and 0.06-mil foils (all with a +15-kV bias). The foils formed wedges of a pie through which the beam scattered. The guns generated 30 μA of 16-keV electrons and 40 μA of 85-keV electrons, and the foils scattered the electrons to a spectrum energy of 1 to 85 keV and a current of 3 μA. The resultant spectrum was measured using an electromagnetic electron spectrometer and is indicated by a dashed line on the graph. We generated Spectrum 2, $dN/dE \propto E^{-1}$, and Spectrum 3, $dN/dE \propto E^{-2}$, using this technique with different foil combinations.

Source electron diagnostics consisted of an electromagnetic spectrometer and an array of Faraday cups. The Faraday cups measured 4 cm deep and had an entrance aperture measuring 1.2 cm^2. The Faraday cups were positioned at eight points around the sample. If viewed from the gun end of the chamber the cups were located at 12 o'clock, 3 o'clock, 6 o'clock, and 9 o'clock. At each of the four dialed positions, one cup rested close to the sample and another near the edge of the back blowoff plate (see cross-sectional view in Fig. 1). The spectrometer was used to measure the electron energy distribution during spectral tests. Sample charge diagnostics included an electrostatic voltmeter (ESV; details of which may be found in Ref. 2). Discharge diagnostics consisted of a back blowoff plate, situated between the samples and the chamber door, a blowoff liner spanning the distance between the samples and the electron guns, and a substrate disc clamped to the dielectric samples. Figure 1 shows a side view of the diagnostics and Figure 3 shows a conceptual view. The blowoff liner, back plate, and substrate were electrically connected to ground using numerous resistors connected in parallel to form a low-inductance 1-Ω path to ground (twenty 20-Ω resistors for the blowoff liner, eighty-two 82-Ω resistors for the back blowoff plate and twelve 12-Ω resistors for the substrate). Electrons that blew off the sample produced negative current signals on the two blowoff diagnostics and produced a positive signal on the substrate.

The signals produced on the substrate and liners during a discharge event were monitored using Tektronix 7903 oscilloscopes with 7A19, 50-Ω impedance plug-ins. Data channels were time-tied. All the scopes were triggered simultaneously using a pulse sent from a fiducial generator and fan-out box. The fiducial generator was triggered only when discharge currents, as measured on the substrate, were greater than a preset value (generally selected between 0.02 and 0.5 A). A sample of a time-tied discharge event is shown in Figure 4. All graphs presented in this paper key on the substrate current trace.

3. GENERAL TRENDS IN THE DATA

This section discusses the charge and discharge properties that the dielectric samples as a unit exhibited in the four types of electron tests - monoenergetic low,

monoenergetic mid, dual, and spectrum. It compares the results obtained in each test in terms of sample surface potential, discharge amplitude, and time rate of change of a discharge. The samples consisted of 5 sheet dielectric samples - Teflon (5 mil); OSR (8 mil), Kapton (2 mil), perforated Kapton (5 mil), and Mylar (2 mil); and 2 porous dielectric samples - Alphaquartz and a "nude" STS (Space Transportation Systems) tile. The OSR sample was formed from an array of 20 cells and constituted a segmented dielectric sample and the perforated Kapton sample had a repeating hole pattern in the form of squares spaced every 0.9 cm. The "nude" STS tile had no thermal paint and since electrons of energy 100 keV or less cannot penetrate the thermal paint that exists on actual shuttle tile, the results should not be extrapolated to anticipated space shuttle environments.

3.1 LOW-ENERGY ELECTRON TEST RESULTS

Several interesting results were noted when exposing the seven samples to low-energy electrons. First, none of the samples discharged when exposed to electrons of energy 8 keV or less. Second, the nonporous samples exhibited two distinct types of discharges: (1) small discharges with $I < 5$ A and $\tau_{FWHM} < 20$ ns accompanied by no change in the sample surface potential, and (2) large discharges with $I >> 10$ A and $\tau_{FWHM} > 300$ ns accompanied by a change in the samples's surface potential equal to or exceeding half the initial potential. Third, the porous samples exhibited only small discharges $I < 5$ A and $\tau_{FWHM} < 50$ ns. Fourth, the porous samples discharged with surface potentials at or less than -1.1 kV and the nonporous samples had to reach surface potentials exceeding -5.5 kV prior to discharge. Finally, all samples displayed a discharge equal to their worst-case discharge current when exposed to 25-keV electrons. Table 1 summarizes the worst-case discharge characteristics of the seven samples. Except for the Kapton sample the worst-case discharge amplitudes agree with results found in previous studies. The Kapton sample produced its few discharges only when exposed to 25-keV electrons at 16 nA/cm^2; otherwise, exposed to an electron flux of 1 nA/cm^2 the Kapton sample produced small discharges $I < 5$ A. All other samples could produce their worst-case discharges when exposed to electrons at fluxes of 1 nA/cm^2 or less.

As noted in the table, the perforated Kapton sample produced a larger discharge than the nonperforated Kapton sample. This result should be alarming; especially since the perforated Kapton sample was developed to ward off discharges better than the nonperforated Kapton sample. Moreover, Mulenberg and Robinson noted this discharge characteristic several years ago (Ref. 8). (These data reaffirm their findings.)

The Kapton samples displayed a general lack of ability to discharge. Published literature pertaining to Kapton testing in the laboratory misleads one into believing that all Kapton samples discharge [Verdin 1980 (Ref. 9), Balmain 1980 (Ref. 10), Balmain 1979 (Ref. 3), Adamo 1980 (Ref. 11)]. Every article speaks of large discharges observed on Kapton samples and only one article [Treadaway, et al., 1977 (Ref. 2)] mentions any difficulty in making a sample discharge. Balmain (Ref. 12) confirms the misrepresentation of the discharging ability of Kapton found in the literature. Balmain has acquired several samples of Kapton that refuse to discharge. Stevens (Ref. 13) has also come across numerous Kapton samples that will not discharge. In fact, in a recent experiment performed by Leung and Plamp (Ref. 14), after they failed to make their sample discharge by electron exposure alone, Leung enlisted the help of Stevens who in turn suggested that a hole be punched through the sample to help it to produce discharges (Ref. 15). The

experience of these researchers shows that there exist batches of Kapton that would make excellent spacecraft insulators because of their ability to ward off discharges.

3.2 MID-ENERGY ELECTRON TEST RESULTS

The general response of the samples was fairly insensitive to the energy of electrons, provided the electrons did not penetrate entirely through the sample (electrons greater than 80 keV could penetrate the 2-mil Kapton and 2-mil Mylar samples). Figures 5, 6, 7, and 8 summarize the discharge amplitude (two figures), I, rate of rise of the pulse, dI/dt, and surface potential prior to discharge, V_i, all as a function of incident-electron energy.

Pulse amplitudes on the OSR, Mylar, Alphaquartz, and STS tile show no dependence on incident-electron energy. Despite the fact that 100-keV electrons (50 keV for Mylar) bury themselves much deeper than 16-keV electrons, the samples produced a similar discharge at both extremes in energy. Even though the perforated Kapton and Teflon samples show a marked decrease in discharge amplitude at 80 keV and 100 keV, they too show little effect on pulse amplitude or shape from 15 keV to 75 keV, despite the fact that for Kapton the practical range of 25-keV electrons is 8×10^{-4} cm and for 75-keV electrons it is 5.4×10^{-3} cm (6×10^{-4} cm and 4.4×10^{-3} cm for Teflon)(Ref. 7).

Figure 7 shows that the rate of rise of the pulse, dI/dt, is certainly independent of energy, and appears to be independent of sample. All samples except the Alphaquartz sample had $dI/dt \approx 5 \times 10^{8}$ A/s. The Alphaquartz sample had $dI/dt \approx 5 \times 10^{6}$ A/s. Large discharges and small discharges had similar dI/dt. Furthermore, visual observations made of the discharges on Teflon indicate that a bright flash from a localized spot can be associated with both types of discharges (where large discharges have a dimmer and very broad flash that covers the entire sample together with the bright localized arc). These observations may indicate that (1) a similar discharge process initiates both small and large discharges, and (2) the discharge process may be the same sample by sample.

Figure 8 shows the sample surface potential prior to discharge. Note that the predischarge surface potential remains the same or slightly increases for increasing electron energy. One would think that if the bulk electric field determines the potential at breakdown, then the closer the charge is buried to a grounded substrate, the lower the potential required to equal a given field and hence initiate a discharge. The data disagree with this simple model. Despite the difference between the practical range of 16-keV electrons (2.4×10^{-4} cm) and 100-keV electrons (6.4×10^{-3} cm) on the 2.16×10^{-2} cm thick OSR sample, the potential at discharge went from -6.5 kV for 16-keV exposure to -12 kV at 100-keV exposure (instead of something less negative than -6.5 kV). As a further note, the sheet dielectric materials of Mylar, Teflon, and Kapton had breakdown potentials close to 10^{6} V/cm breakdown threshold electric field times the sample's thickness. The perforated Kapton and OSR sample produced discharges at potentials approximately one quarter of the bulk field threshold times sample thickness. Finally, the porous samples displayed discharges at very low potentials compared to their thickness and any supposed net threshold field.

3.3 COMBINED LOW- AND MID-ENERGY ELECTRON TEST RESULTS

Figures 6, 7, and 8 also summarize data obtained from combined energy electron exposure tests (see left-hand portions of the graphs).

The pulse amplitudes observed in the combined energy tests are smaller than the pulses found in monoenergetic tests. In fact, the small discharges, $I < 5$ A, observed in the monoenergetic tests appear identical to most discharges seen in the combined energy tests. These discharges have $I < 5$ A and $\tau_{FWHM} < 20$ ns.

Despite the small pulse amplitude, Figure 7 shows that dI/dt for the combined-energy produced discharges remains near 10^8 A/s. Moreover, the discharges observed in this electron environment occurred when the samples had a much reduced surface potential compared to monoenergetic tests. The Teflon, perforated Kapton and STS tile produced discharges in all combined-energy electron environments, even when their surface potentials were as low as -1 kV (0 kV for the STS tile). The Mylar and OSR samples produced discharges when surface potentials were less negative than -5 kV, but required a structured potential surface with a variation of 1 kV or greater across the plane of the sample. The Teflon and perforated Kapton samples did not require any potential structuring in order to produce discharges. The Kapton and Alphaquartz samples did not discharge in a combined-energy electron environment when their surface potential was kept less negative than -5 kV.

A simple qualitative model can explain the reduced potentials at discharge for combined low- and mid-energy electron exposures compared to the discharge potentials with mid-energy electrons alone. Leung, et al. (Refs. 16 and 17) have demonstrated experimentally that the surface potential of a dielectric sample can be varied over a considerable range by irradiating with electrons of two energies. Moreover, they showed that the surface potential is a strong function of the secondary electron-emission properties of the test dielectric due to the low-energy incident electrons. Where only mid-energy electrons are used, the charge is stopped at some average depth, a fraction of its practical range, R_p, beneath the surface of the sample. An electric field, established between the buried charge and the sample substrate, increases as more charge is deposited. If the breakdown threshold electric field is exceeded at a critical point in the sample (not necessarily the bulk of the material), then a discharge will occur. The surface potential of the sample at such an instance reflects the electric field integrated over a line path from the substrate to the charge layer.

When low-energy electrons are combined with the mid-energy electrons, the trajectories of the mid-energy electrons will not be affected significantly so they will again be deposited at a depth R_p into the sample. However, as the surface potential increases due to the trapped electrons, the low-energy electrons will reach the second crossover for secondary electron emission from the surface. Thereafter, the low-energy electrons will emit more than one electron per incident electron and the surface of the sample will become positively charged. The electric field inside the dielectric will then consist of a positive field from the substrate to the trapped mid-energy electrons and a negative field from those trapped electrons to the sample surface. The surface potential will then be the line integral of these two fields. A discharge could occur if either of the two fields exceeds the threshold field at some critical point.

3.4 SPECTRAL-ENERGY TEST RESULTS

Figures 6, 7, and 8 also summarize spectral test discharge characteristics of the four samples tested (Teflon, OSR, Alphaquartz, and Kapton), this time on the right-hand side of the graph. Several important trends are noted in the figures.

a. The worst-case discharges observed in the spectral tests, particularly the dN/dE ∝ const. (Spectrum 1), equals the worst-case discharges seen in monoenergetic tests.

b. The OSR and Tefon samples produced predominantly two types of discharges: large discharges with $I \gg 10$ A and $\tau_{FWHM} > 300$ ns, and small discharges with $I < 5$ A and $\tau_{FWHM} < 20$ ns.

c. A rarely seen mid-size discharge was observed and after close scrutiny of the monoenergetic test results we have concluded two things: (1) the mid-size discharges appeared in monoenergetic tests as well, and (2) the mid-size discharge is accompanied by a structured surface potential before discharge. For the Teflon sample, the mid-size discharge has a mid-size amplitude $5 \text{ A} < I < 100$ A and mid-size pulse width $20 \text{ ns} < \tau_{FWHM} < 300$ ns. Figures 9 and 10 summarize these data for the Teflon sample. Note that most discharges on Teflon are large or small, but that there are only a few discharges with pulse amplitudes between 5 and 100 A.

It is also interesting to note that Balmain's discharge area scaling laws (Ref. 18) may be applied here in order to infer the area of a discharge site. Balmain found three laws: $I \propto A^{1/2}$, $\tau_{FWHM} \propto A^{1/2}$, and $I/\tau_{FWHM} = \text{const.}$ (where A was the area of the sample and in this case represents the area of the discharge site). Assuming that the pulse duration is determined by the propagation time of an arc across the sample, i.e., $A = \pi(\tau V)^2$ where $V \propto \sqrt{I/\tau}$ is the discharge propagation velocity, Balmain found $V \approx 3 \times 10^7$ cm/s. Balmain's measured value for I/τ was 2.8×10^8 A/s. From the dashed line in Figure 10, values for I/τ are seen to span the range 7×10^7 to 7×10^8 A/s. This yields an average propagation speed of 3.5×10^7 cm/s. Thus, a 5-ns wide pulse would have an implied discharge site area of 0.1 cm^2. The rarely observed mid-size discharges would have discharge areas covering up to one half the sample's area, and the large discharge pulses, with $\tau_{FWHM} \sim 300$ ns, appear to cover nearly the entire surface area.

d. The substorm-like spectral tests, Spectrum 3 tests, produced discharges only on the Teflon sample. However, it kept all samples from charging more negatively than -5 kV. Thus, the effect of secondary electron emission is important in determining the sample's potential.

e. The Alphaquartz and Kapton samples exhibited the charge and discharge characteristics that they exhibited in all their monoenergetic tests. Both samples charged to only a few kV when exposed to electrons at fluxes less than 1 nA/cm^2, and both samples warded off any large discharges. If a material selection were based on these tests alone, the Kapton and Alphaquartz samples would make excellent spacecraft charge and discharge control materials.

4. CONCLUSIONS

a. For worst-case testing of satellite dielectrics, monoenergetic 25-keV electron beams should be sufficient to bound the amplitude and pulse width of discharges anticipated in both enhanced and natural space environments without significant over or understress.

b. Dual-energy and spectral-energy electron environments can generate sample discharges while maintaining low surface potentials. Low-energy electrons can cause enough secondary emission to keep the surface potential low while the mid-energy electrons deposit enough charge to produce discharges. This result should help

explain why and how low surface potentials can be measured at the time of discharge on operational satellites.

c. Two distinct types of discharges are noted: small discharges with small amplitude and pulse width ($I < 5$ A and $\tau < 20$ ns), and large discharges with large pulse widths ($I >> 10$ A and $\tau > 300$ ns). The large discharges have been well characterized in previous studies. These discharges are accompanied with large changes in surface potential and act to cleanse the sample of stored charge. The small discharges have gone relatively unmentioned in previous work and appear to not change the sample's surface potential nor release much of the stored charge (much less than 0.1%). The small discharges may give way to the large discharges when the appropriate environmental conditions are met (namely surface potentials exceeding negative 5 kV).

d. For the thin dielectric samples that were tested, the Alphaquartz and nonperforated Kapton samples appear to be best suited to ward off large discharges. The samples produced only small narrow discharges when exposed to realistic fluxes (less than 0.3 nA/cm^2). A well documented data base found in the literature supports our observation that Alphquartz does not produce any charge-cleansing large discharges. The open literature, however, reports that Kapton produces large discharges. Under reexamination, though, many researchers confirm that it is sometimes impossible to produce large discharges on selected Kapton samples.

REFERENCES

1. For a review of the literature, see Spacecraft Charging Technology, 1977, 1978, and 1980, NASA Conference Publication, NASA TMX-73537, 2071, 2181, respectively. Also see December issue (No. 6) of the IEEE Trans. Nucl. Sci. for the last several years.

2. M. J. Treadaway, et al. "Effects of Laboratory Simulation Parameters on Spacecraft Dielectric Discharges," JAYCOR Report J200-79-155, July 1979.

3. K. G. Balmain and G. R. Dubois, "Surface Discharges on Teflon, Mylar, and Kapton," IEEE Trans. Nucl. Sci., NS-26, No. 6, December 1976, p. 5146.

4. P. Mizera, et al., "Spacecraft Charging in the Spring of 1981," Aerospace Report TDR-0081 (6508-05)-01, Sept. 30, 1981.

5. N. J. Stevens, "Analytical Modeling of Satellites in Geosynchronous Environment," Spacecraft Charging Technology, 1980, NASA Pub. 2182.

6. R. Shaw, et al., "Observations of Electrical Discharges Caused by Differential Satellite-Charging," Spacecraft Charging by Magnetospheric Plasmas, Alan Rosen, Ed., MIT Press, Mass., 1976., p. 61.

7. M. J. Berger and S. M. Seltzer, "Tables of Energy Loss and Ranges of Electrons and Positrons," NASA Report NASA-SP-3021, 1964.

8. A. Mulenberg and P. A. Robinson, Jr., "Conduction through Punctures in Metal-Backed Dielectrics," Spacecraft Charging Technology, AFGL-TR-81-0270, p. 342.

9. D. Verdin, "Electrostatic Discharging Behavior of Kapton Irradiated with Electrons," Spacecraft Charging Technology - 1980, AFGL-TR-81-0270, p. 96.

10. K. G. Balmain and W. Hirts, "Dielectric Surface Discharges: Effects of Combined Low-Energy and High-Energy Incident Electrons," Spacecraft Charging Technology - 1980, AFGL-TR-81-0270, p. 115.

11. R. C. Adamo and J. E. Nanevicz, "Preliminary Comparison of Material Charging Properties Using Single-Energy and Multienergy Electron Beams," Spacecraft Charging Technology - 1980, AFGL-TR-81-0270, p. 129.

12. K. Balmain, private communication, 1983.

13. N. J. Stevens, private communication, 1983.

14. P. Leung and G. Plamp, "Characteristics of RF Resulting from Dielectric Discharges," IEEE Trans. Nucl. Sci., NS-29, No. 6, December 1982, p. 1610.

15. P. Leung and G. Plamp, private communication, 1983.

16. M. S. Leung, et al., "Effects of Secondary Electron Emisssion of Charging," Spacecraft Charging Technology - 1980, NASA Pub. 2182.

17. P. F. Mizera, M. S. Leung, and H. K. A. Kan, Laboratory and Space Results from the SSPM Experiment, Aerospace Report No. TOR-0081 (6505-02)-3, July 15, 1981.

18. K. G. Balmain, "Scaling Laws and Edge Effects for Polymer Surface Discharges," Spacecraft Charging Technology - 1978, AFGL-TR-79-0082, p. 646.

Table 1. Characteristics of worst-case discharges

		OSR #84	Teflon #863	Perforated Kapton #638	Kapton #136	Mylar #139	Alphaquartz #904	STS tile #988
V_i(kV)	Potential prior to discharge	10.5	20	6.1	15	13.7	5.2	0
V_f(kV)	Potential following discharge	2	3.3	0.9	--	1.4	5.2	0
$\langle\Delta V\rangle$ (kV)	$(V_i - V_f)$ average change in surface potential	8.5	16.7	5.2	--	12.3	0	--
I_{SUB}(A)	Peak discharge current	70	300	100	12.5	425	0.3	0.35
τ_{FWHM}(ns)	Full-width at half-max. of I_{SUB} vs. time	300	280	200	800	700	100	20
dI_{SUB}/dt (A/s)	Peak change in current measured with respect to time	3.5×10^8	1×10^9	1×10^9	5×10^8	1.2×10^9	5×10^6	4×10^8

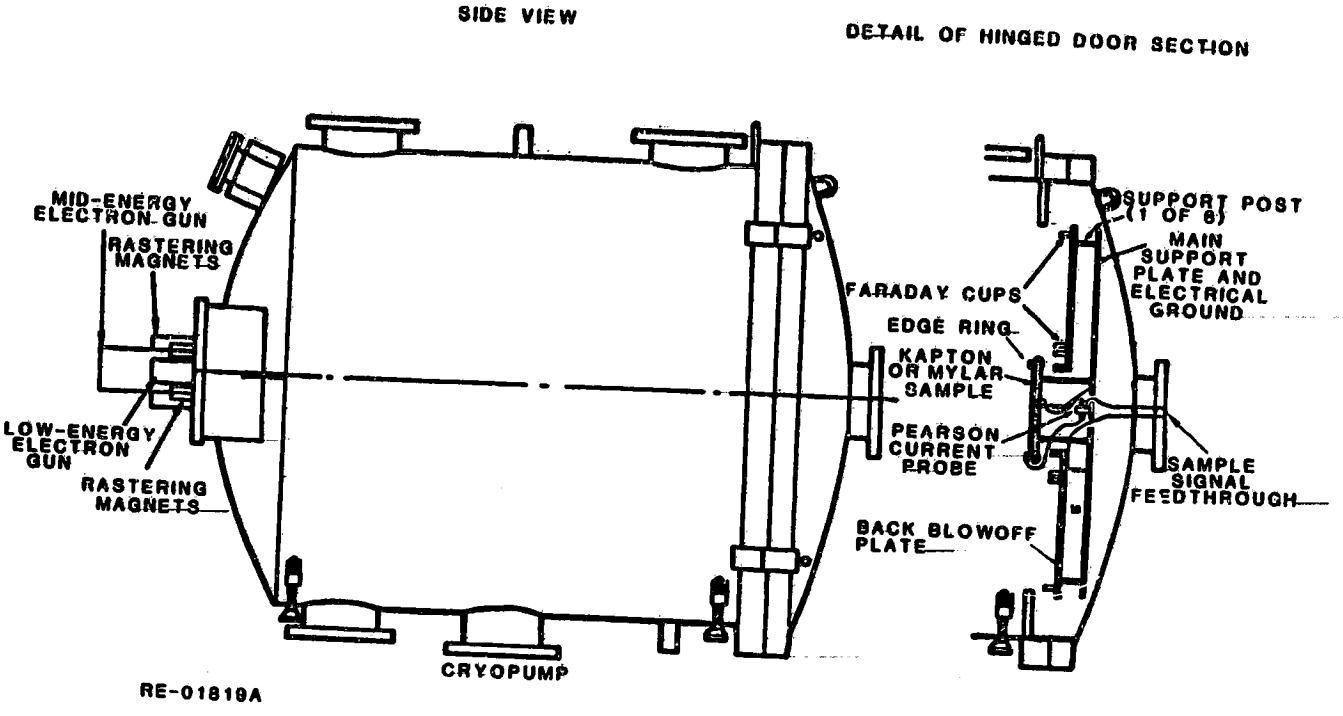

Figure 1. Diagram of the test configuration

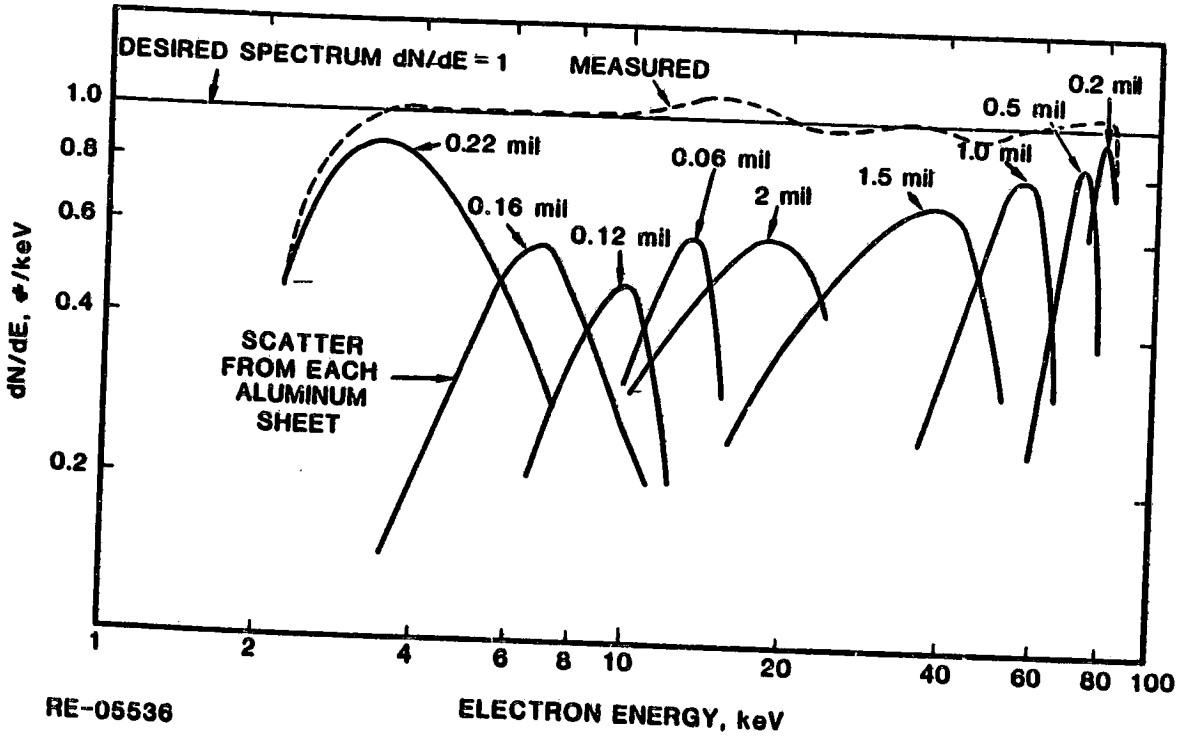

Figure 2. Energetic electron spectrum from 1 to 100 keV

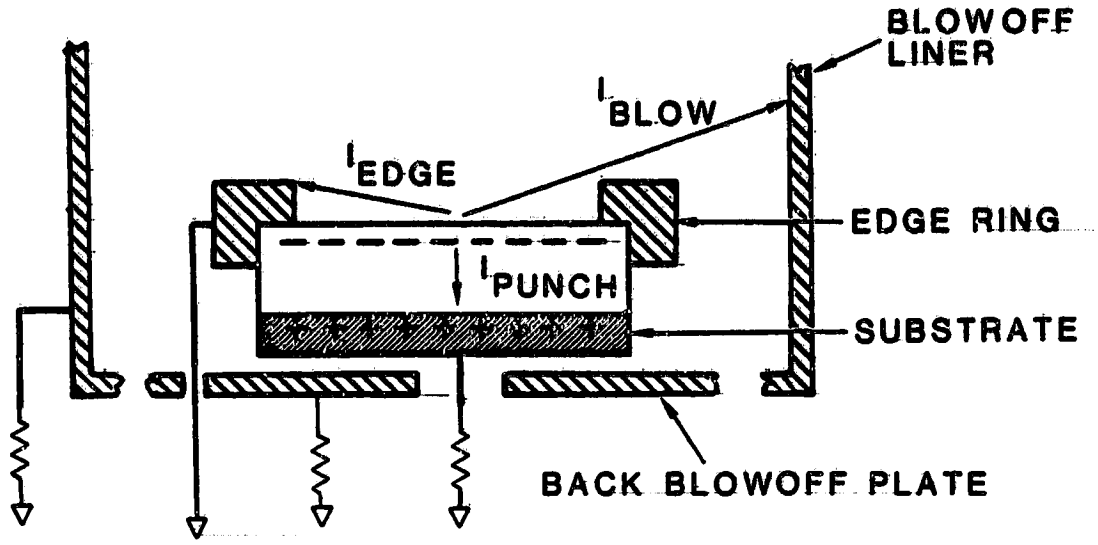

RE-02529B

Figure 3. Diagram of charge motion and discharge diagnostics

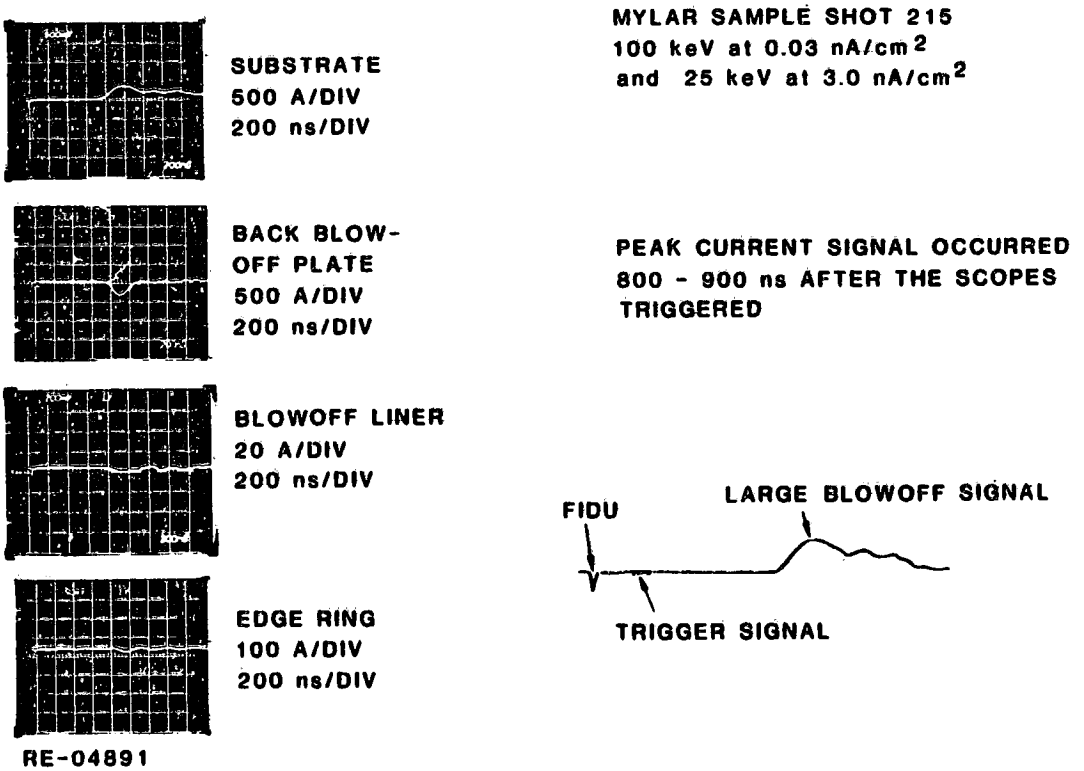

Figure 4. Time-tied discharge event on Mylar in combined-energy environment

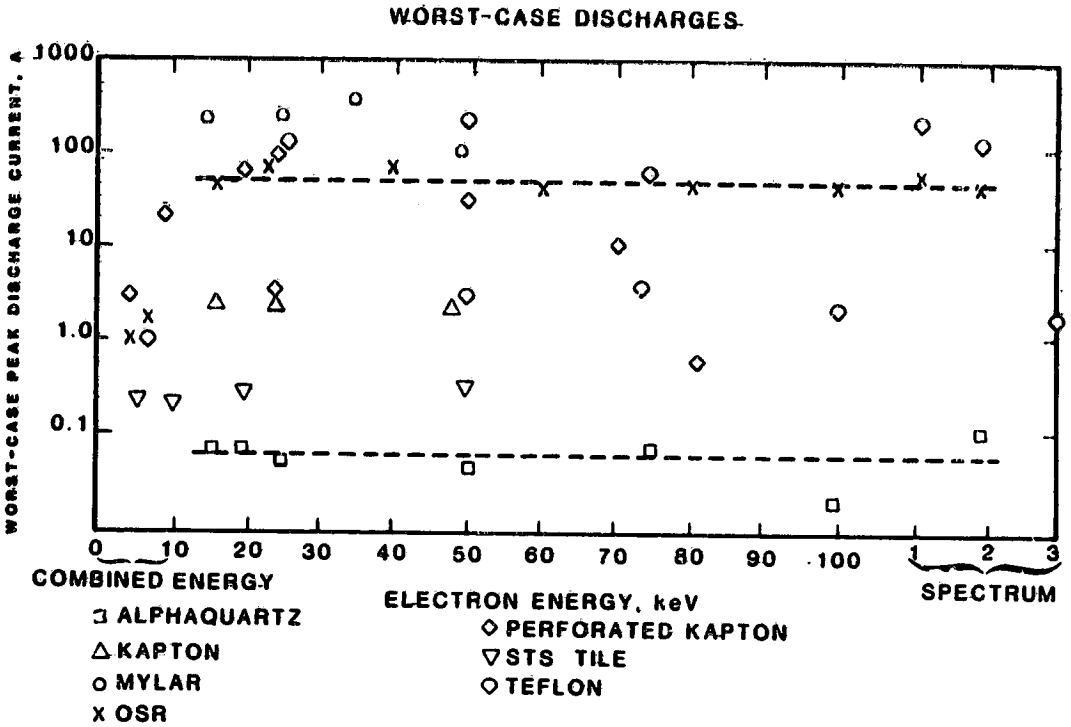

Figure 5. Worst-case discharges observed in the four testing environments

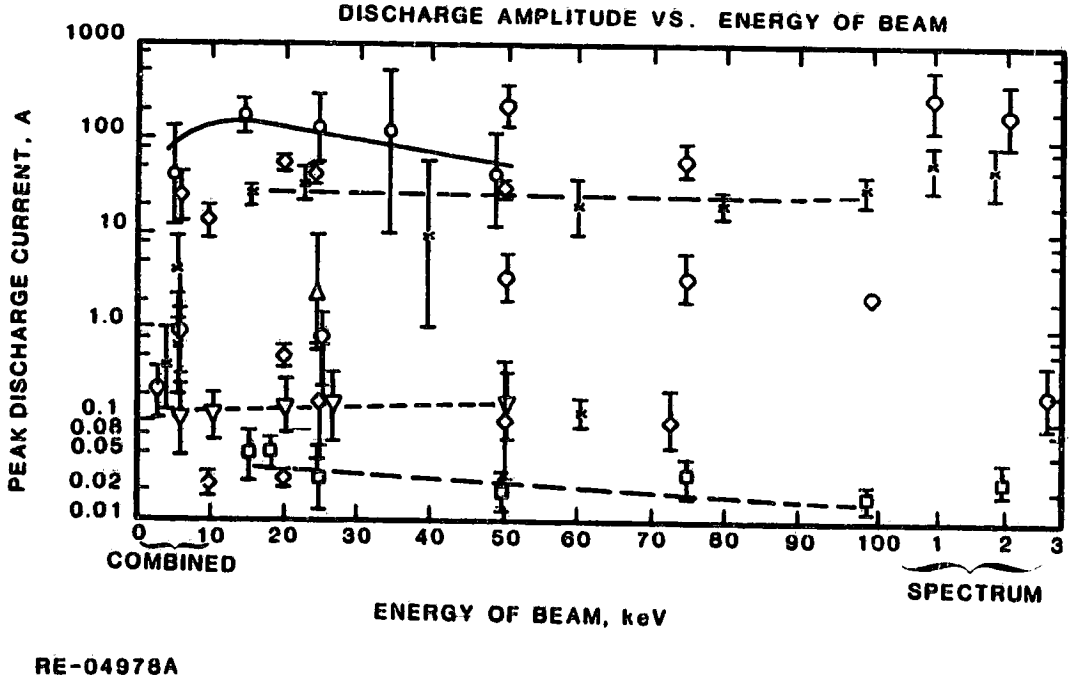

Figure 6. Compilation of all data: peak discharge currents vs. electron energy (same symbol legend as Figure 5)

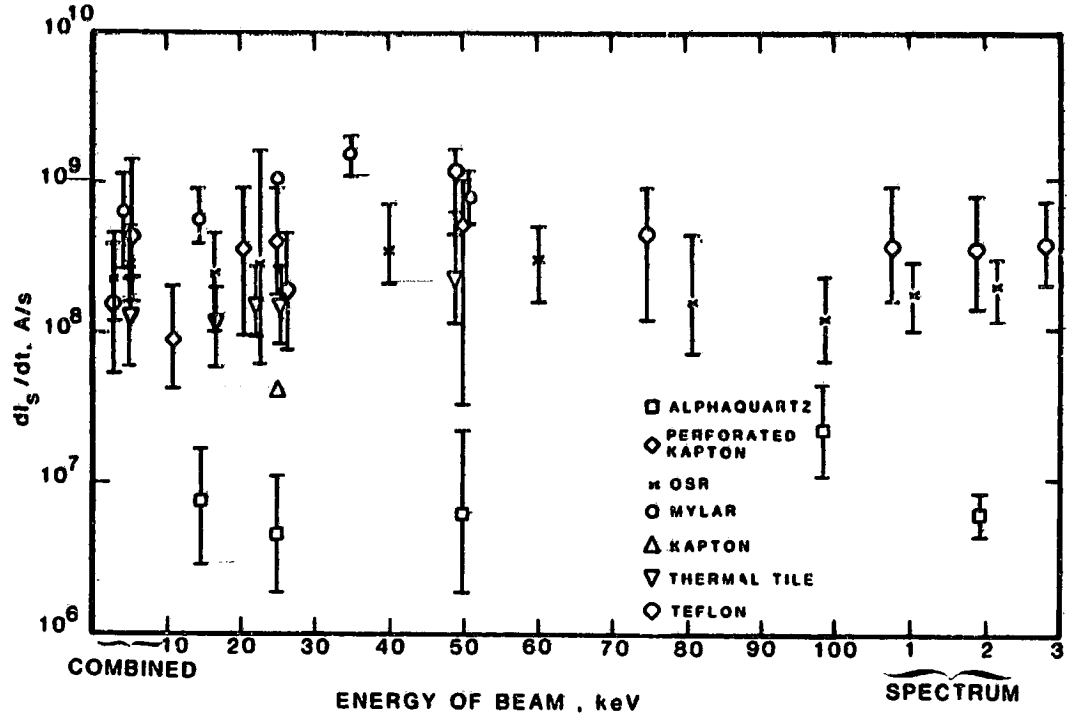

RE-04874A

Figure 7. Compilation of all data: dI/dt vs. electron energy (same symbol legend as Figure 5)

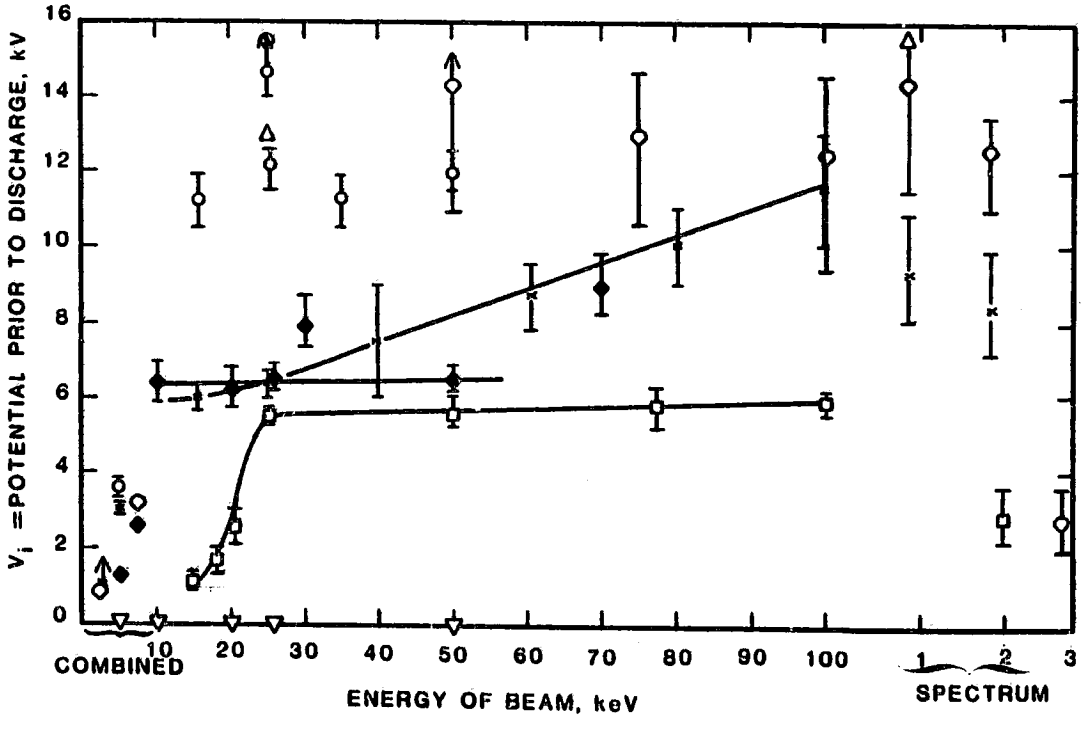

RE-04876A

Figure 8. Compilation of all data: potential of sample prior to discharge vs. electron energy (same symbol legend as in Figure 5)

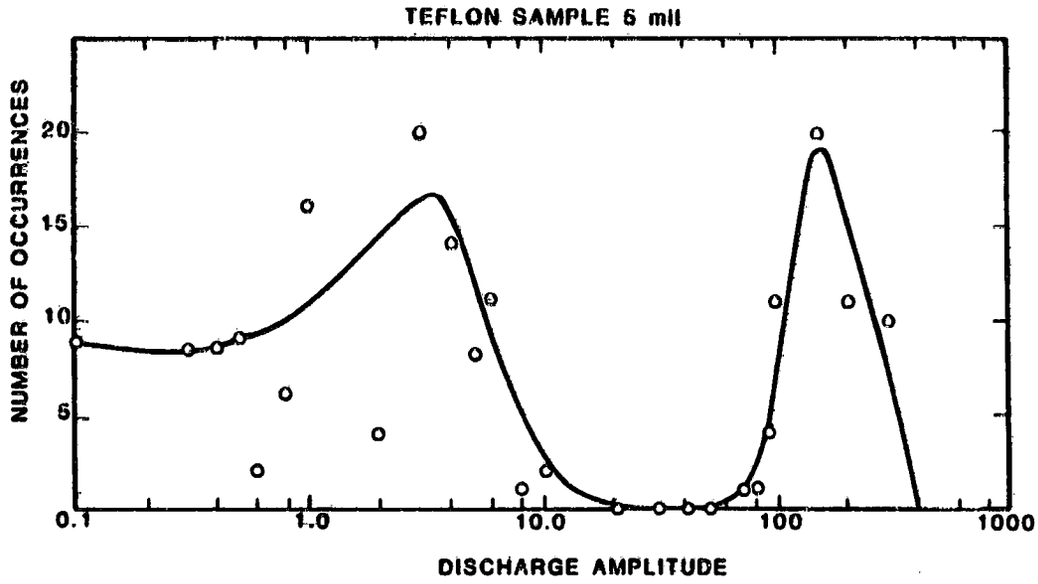

RE-05937

Figure 9. Number of discharge occurrences at a specific amplitude: depicts void of 10 to 100 A discharges

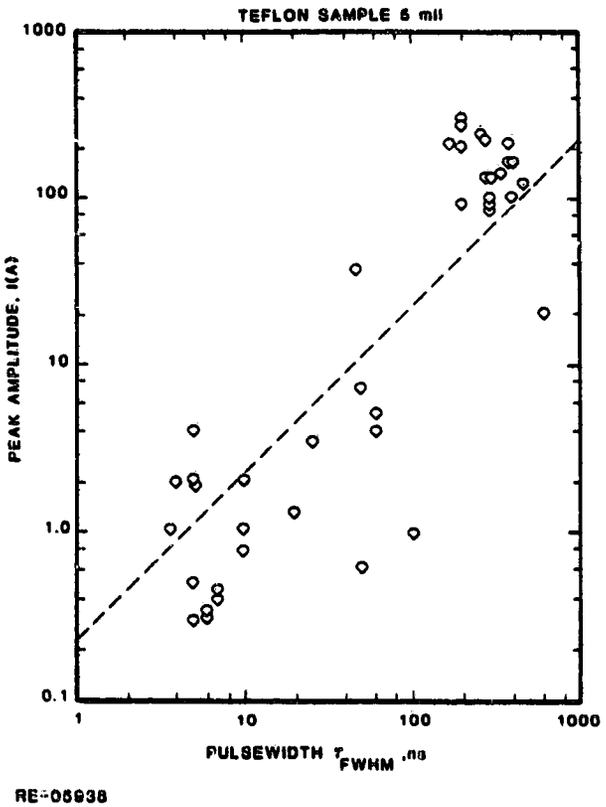

RE-05938

Figure 10. Plot of discharge pulse amplitude vs. pulse width showing a lack of 60 to 200 ns pulse widths